# 512QAM Nyquist sinc-pulse transmission at 54 Gbit/s in an optical bandwidth of 3 GHz

**R. Schmogrow,[1,*] D. Hillerkuss,[1] S. Wolf,[1] B. Bäuerle,[1] M. Winter,[3] P. Kleinow,[1] B. Nebendahl,[4] T. Dippon,[4] P. C. Schindler,[1] C. Koos,[1,2] W. Freude,[1,2] and J. Leuthold[1,2]**

[1]*Institute of Photonics and Quantum Electronics (IPQ), Karlsruhe Institute of Technology (KIT), Karlsruhe, Germany*
[2]*Institute of Microstructure Technology (IMT), Karlsruhe Institute of Technology (KIT), Karlsruhe, Germany*
[3]*Polytec GmbH, Waldbronn, Germany*
[4]*Agilent Technologies, Boeblingen, Germany*
[*]*rene.schmogrow@kit.edu*

**Abstract:** We demonstrate for the first time transmission of 54 Gbit/s and 48 Gbit/s over 44 km and 150 km, respectively, utilizing an optical bandwidth of only 3 GHz. We used polarization division multiplexed 512QAM and 256QAM modulation formats in combination with Nyquist pulse shaping having virtually zero roll-off. The resulting spectral efficiencies range up to 18 bit/s/Hz and 16 bit/s/Hz, respectively. Taking into account the overhead required for forward error correction, the occupied signal bandwidth corresponds to net spectral efficiencies of 14.4 bit/s/Hz and 15 bit/s/Hz, which could be achieved in a wavelength division multiplexed network without spectral guard bands.



**OCIS codes:** (060.4510) Optical communications; (060.1660) Coherent communications.

## References and links

1. G. Bosco, A. Carena, V. Curri, P. Poggiolini, and F. Forghieri, "Performance limits of Nyquist-WDM and CO-OFDM in high-speed PM-QPSK systems," IEEE Photon. Technol. Lett. **22**(15), 1129–1131 (2010).
2. R. Schmogrow, M. Winter, M. Meyer, D. Hillerkuss, S. Wolf, B. Baeuerle, A. Ludwig, B. Nebendahl, S. Ben-Ezra, J. Meyer, M. Dreschmann, M. Huebner, J. Becker, C. Koos, W. Freude, and J. Leuthold, "Real-time Nyquist pulse generation beyond 100 Gbit/s and its relation to OFDM," Opt. Express **20**(1), 317–337 (2012).
3. H. Nyquist, "Certain topics in telegraph transmission theory," Trans. Am. Inst. Electr. Eng. **47**, 617–644 (1928).
4. N. Bergano, "Wavelength division multiplexing in long-haul transmission systems," *Frontiers in Optics*, OSA Technical Digest Series (Optical Society of America, 2004), paper FMF4.
5. C. A. Brackett, "Dense wavelength division multiplexing networks: principles and applications," IEEE J. Sel. Area. Commun. **8**(6), 948–964 (1990).
6. B. Zhu, L. E. Nelson, S. Stulz, A. H. Gnauck, C. Doerr, J. Leuthold, L. Gruner-Nielsen, M. O. Pedersen, J. Kim, and R. L. Lingle, Jr., "High spectral density long-haul 40-Gb/s transmission using CSRZ-DPSK format," J. Lightwave Technol. **22**(1), 208–214 (2004).
7. G. Bosco, V. Curri, A. Carena, P. Poggiolini, and F. Forghieri, "On the performance of Nyquist-WDM terabit superchannels based on PM-BPSK, PM-QPSK, PM-8QAM or PM-16QAM subcarriers," J. Lightwave Technol. **29**(1), 53–61 (2011).
8. D. Hillerkuss, R. Schmogrow, M. Meyer, S. Wolf, M. Jordan, P. Kleinow, N. Lindenmann, P. Schindler, A. Melikyan, X. Yang, S. Ben-Ezra, B. Nebendahl, M. Dreschmann, J. Meyer, F. Parmigiani, P. Petropoulos, B. Resan, A. Oehler, K. Weingarten, L. Altenhain, T. Ellermeyer, M. Moeller, M. Huebner, J. Becker, C. Koos, W. Freude, and J. Leuthold, "Single-laser 32.5 Tbit/s Nyquist WDM transmission," submitted to Opt. Express.
9. J. C. Cartledge, J. D. Downie, J. E. Hurley, A. S. Karar, Y. Jiang, and K. Roberts, "Pulse shaping for 112 Gbit/s polarization multiplexed 16-QAM signals using a 21 GSa/s DAC," Opt. Express **19**(26), B628–B635 (2011).
10. W. Shieh, H. Bao, and Y. Tang, "Coherent optical OFDM: theory and design," Opt. Express **16**(2), 841–859 (2008).
11. R. Schmogrow, M. Winter, D. Hillerkuss, B. Nebendahl, S. Ben-Ezra, J. Meyer, M. Dreschmann, M. Huebner, J. Becker, C. Koos, W. Freude, and J. Leuthold, "Real-time OFDM transmitter beyond 100 Gbit/s," Opt. Express **19**(13), 12740–12749 (2011).
12. M. Sjödin, P. Johannisson, H. Wymeersch, P. A. Andrekson, and M. Karlsson, "Comparison of polarization-switched QPSK and polarization-multiplexed QPSK at 30 Gbit/s," Opt. Express **19**(8), 7839–7846 (2011).
13. S. Okamoto, K. Toyoda, T. Omiya, K. Kasai, M. Yoshida, and M. Nakazawa, "512 QAM (54 Gbit/s) coherent optical transmission over 150 km with an optical bandwidth of 4.1 GHz," in *36th European Conference and Exhibition on Optical Communication (ECOC 2010)*, paper PD2.3.
14. S. D. Personick, "Receiver design for digital fiber optic communication systems, I," Bell Syst. Tech. J. **52**, 843–874 (1973).

#161525 - $15.00 USD Received 13 Jan 2012; revised 18 Feb 2012; accepted 29 Feb 2012; published 5 Mar 2012

15. R. Schmogrow, S. Wolf, B. Baeuerle, D. Hillerkuss, B. Nebendahl, C. Koos, W. Freude, and J. Leuthold, "Nyquist frequency division multiplexing for optical communications," submitted to Conference on Lasers and Electro-Optics 2012.
16. Z. Dong, J. Yu, H. C. Chien, N. Chi, L. Chen, and G. K. Chang, "Ultra-dense WDM-PON delivering carrier-centralized Nyquist-WDM uplink with digital coherent detection," Opt. Express **19**(12), 11100–11105 (2011).
17. X. Zhou, L. Nelson, P. Magill, B. Zhu, and D. Peckham, "8x450-Gb/s, 50-GHz-spaced, PDM-32QAM transmission over 400km and one 50GHz-grid ROADM," in *Optical Fiber Communications Conference*, OSA Technical Digest (CD) (Optical Society of America, 2011), paper PDPB3.
18. M. S. O'Sillivan, K. Roberts, and C. Bontu, "Electronic dispersion compensation techniques for optical communication systems," in *31st European Conference and Exhibition on Optical Communication (ECOC 2005)*, paper Tu3.2.1.
19. C. Xia and W. Rosenkranz, "Electrical dispersion compensation for different modulation formats with optical filtering," in *Optical Fiber Communication Conference*, OSA Technical Digest (CD) (Optical Society of America, 2006), paper OWR2.
20. B. Szafraniec, B. Nebendahl, and T. Marshall, "Polarization demultiplexing in Stokes space," Opt. Express **18**(17), 17928–17939 (2010).
21. C. E. Shannon, "A mathematical theory of communication," Bell Syst. Tech. J. **27**, 623–656 (1948).
22. Telecommunication standardization sector of International telecommunication union (ITU-T), Transmission system and media, digital system and networks G.975.1.
23. T. Mizuochi, "Recent progress in forward error correction and its interplay with transmission impairments," IEEE J. Sel. Top. Quantum Electron. **12**(4), 544–554 (2006).
24. R. Schmogrow, B. Nebendahl, M. Winter, A. Josten, D. Hillerkuss, S. Koenig, J. Meyer, M. Dreschmann, M. Huebner, C. Koos, J. Becker, W. Freude, and J. Leuthold, "Error vector magnitude as a performance measure for advanced modulation formats," IEEE Photon. Technol. Lett. **24**(1), 61–63 (2012).
25. T. Kremp and W. Freude, "Fast Split-Step Wavelet Collocation Method for WDM System Parameter Optimization," J. Lightwave Technol. **23**(3), 1491–1502 (2005).
26. K.-P. Ho, "Error probability of DPSK signals with cross-phase modulation induced nonlinear phase noise," IEEE J. Quantum Electron. **10**(2), 421–427 (2004).

## 1. Introduction

Sinc-shaped Nyquist pulses [1,2] are attractive to achieve high spectral efficiencies. They overlap in time but follow each other at such a symbol period $T_s$ so that they do not interfere according to the Nyquist inter-symbol interference (ISI) criterion. With this condition met, no inter-symbol crosstalk occurs. The resulting signal spectrum has an ideal rectangular shape. Therefore, sinc-shaped signals require the minimum Nyquist bandwidth [3], a fact which is beneficial in networks with multi-carrier or wavelength division multiplexing (WDM) as is common today [4–6]. The rectangular spectral shape allows decreasing the WDM channel frequency spacing up to the point where the spacing equals the symbol rate. This scenario is known as Nyquist WDM [7,8]. Sinc-shaped Nyquist signals are also often described by a so-called "zero roll-off" characteristic of raised cosine-shaped spectra [9].

Nyquist pulse shaping has much in common with orthogonal frequency division multiplexing (OFDM) [10,11]. In fact, both are related by a duality principle, so that time and frequency can be simply interchanged [2]. Both Nyquist WDM and OFDM converge towards the same high spectral efficiency (SE) for large OFDM subcarrier and WDM tributary counts, but only Nyquist pulse shaping offers SE advantages for low tributary numbers [2]. Furthermore, Nyquist pulse shaping has some additional advantages: In contrast to OFDM, where subcarriers overlap and thus must be transmitted and processed in synchronism, Nyquist WDM tributaries can be transmitted and processed asynchronously [8]. Further, calculations indicate [2] that Nyquist pulse shaping leads to lower peak-to-average power ratios (PAPR) than OFDM. This could prove advantageous in transmission if nonlinearities play a role, and on reception with a view to the required resolution of the analog-to-digital converters (ADC). Signals having a high PAPR naturally need to be quantized with a high resolution in order to precisely account for large and small amplitudes at the same time.

The spectral efficiency of the transmission can be further increased by using polarization shift keying or polarization division multiplexing (PDM) [12] along with advanced modulation formats such as *M*-ary quadrature amplitude modulation (QAM). Recently, QAM signals in combination with Nyquist pulse shaping using a roll-off factor of $\beta = 0.35$ have been demonstrated. With this technique 54 Gbit/s were transmitted in 512QAM format inside an optical bandwidth of only 4.1 GHz [13]. Appropriate so-called raised-cosine filters are

#161525 - $15.00 USD Received 13 Jan 2012; revised 18 Feb 2012; accepted 29 Feb 2012; published 5 Mar 2012

described in [14, p. 858], and the resulting signal bandwidth $B$ in dependence on the symbol duration $T_s$ (symbol rate 1 / $T_s$) and the roll-off factor $\beta$ follows from

$$B = \frac{1}{T_s}(1+\beta). \tag{1}$$

In this paper we demonstrate a record transmission of 54 Gbit/s within an optical bandwidth of only 3 GHz corresponding to a symbol rate of $1/T_s$ = 3 GBd. This is achieved by employing Nyquist sinc-pulse shaping and a PDM-512QAM format. Our sinc-shaped pulses are basically generated with a roll-off factor of $\beta$ = 0, but technically they are limited to a finite time window of 512 symbol durations $T_s$. Taking that into account, we find from simulations and from Eq. (6) of [2], an actual roll-off $\beta$ = 0.0024. The technique enables Transmission distances of up to 44 km which were reached by employing ultra-large area fiber (ULAF).

We further demonstrate the transmission of 48 Gbit/s in a 3 GHz optical channel over a distance of 150 km in a standard single mode fiber (SSMF) using the Nyquist shaped PDM-256QAM modulation format.

## 2. Experimental setup

The theoretical zero roll-off sinc-shaped Nyquist signal is schematically shown in Fig. 1(a) (green). A single impulse together with its corresponding spectrum is displayed. The measured, ensemble averaged spectrum of a 3 GBd Nyquist sinc-shaped ($\beta$ = 0.0024) signal occupies only a bandwidth of virtually 3 GHz, see Fig. 1(b) and Eq. (1). The power spectrum has been measured with a coherent receiver. The noise floor is due to quantization noise at the transmitter and the receiver, which employed digital-to-analog and analog-to-digital converters with a nominal resolution of 12 bit and 8 bit, respectively. We see an impressive out-of-band suppression of more than 36dB. Therefore linear inter-channel crosstalk between such signals is negligible in WDM networks [8,15].

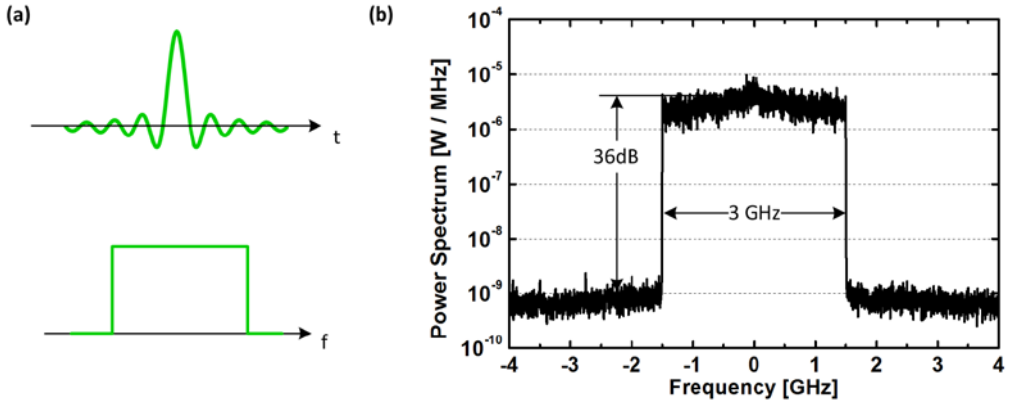


Fig. 1. Schematic of elementary impulse and corresponding spectrum along with signal spectrum in one polarization only. (**a**) sinc-shaped Nyquist impulse and rectangular spectrum. (**b**) Power spectrum of sinc-shaped Nyquist-pulses belonging to a random sequence of constellation points, measured with a coherent receiver and in one polarization. The 14 dB signal bandwidth is 3 GHz for a symbol rate of 3 GBd. The noise floor is due to signal quantization. The out-of-band suppression is more than 36dB.

The experimental Nyquist transmission setup is depicted in Fig. 2. The Nyquist transmitter (Tx) comprises an arbitrary waveform generator (AWG), a narrow linewidth (< 1 kHz) laser source and an optical I/Q-Modulator, see Fig. 2(a). The sinc-shaped Nyquist pulses are generated off-line and stored in an AWG (Agilent M8190A) which has a nominal resolution of 12 bit at a sampling rate of 12 GSa/s, and an electrical bandwidth of 5 GHz. Pseudo random binary sequences (PRBS) show a periodicity of $2^N$–1 whereas memory based signal generators such as AWGs support even-numbered length patterns only. To overcome this

#161525 - $15.00 USD Received 13 Jan 2012; revised 18 Feb 2012; accepted 29 Feb 2012; published 5 Mar 2012

issue when employing standard bit error ratio testers (BERT), a rather short PRBS is replicated until the periodicity of concatenated PRBS patterns agrees with the periodicity required by the memory. For high-order modulation formats such as 256QAM or 512QAM, very long PRBS patterns (e. g. $2^{31}$–1) would be needed in order to assure that all points in the constellation diagram are hit appropriately often. This would require an excessively large AWG memory. Therefore, in this experiment we use random data generated externally by Matlab. We generate new sets of random data for each measurement thereby approximating real data traffic. The generated signals are four-times oversampled to facilitate the removal of periodic spectral repetitions by anti-alias filters. Alternatively, passive optical filters [16] or digital filters with lower oversampling factors can be used to remove spurious spectral tributaries outside of the Nyquist frequency band [17]. The two outputs of the AWG directly drive the in-phase (I) and quadrature (Q) inputs of the optical I/Q-modulator. Nonlinearities introduced by the modulator's sinusoidal transfer function do not significantly broaden the signal spectrum, because the modulator is differentially driven with 700 mV only ($V_\pi \approx 4$ V), and is therefore operated well in its linear regime. A fiber laser (laser 1) with approximately 1 kHz linewidth (nominal wavelength: 1550 nm) serves as a source for the Tx. The inset of Fig. 2(a) shows a schematic eye-diagram of a two-level zero roll-off Nyquist signal. It can be seen that the amplitude of the field is not constant over the symbol duration $T_s$ so that the information can be recovered without error at the point of the maximum eye opening. The tolerance of zero roll-off Nyquist signals with respect to jitter and sampling phase error as well as a novel clock phase recovery algorithm have been discussed in [2].

A PDM signal is generated within the next stage. The optical signal leaving the I/Q-modulator is split onto two arms, delayed by 16 ns in order to de-correlate the signals, and then combined in orthogonal polarizations. Due to the zero roll-off of the signals, an optical bandwidth of only 3 GHz at a symbol rate of 3 GBd is required as seen in Fig. 1(b). As a consequence, virtually all of the signal power is confined to the Nyquist frequency band $B = 1 / T_s$.

During the experiment, we increase the transmission link length in steps up to the full length of 150 km. SMF-28 and OFS ULAF fibers are used. All combinations of SMF-28 and ULAF together with the locations of the EDFAs are shown in Figs. 2(b) and 2(c). At 1550 nm the SMF-28 has a typical loss of 0.19 dB/km with a dispersion of 16.8 ps/nm/km, whereas the ULAF typically attenuates by 0.18 dB/km and comes with a dispersion of 20.2 ps/nm/km. The effective area of the ULAF is specified to be approximately 130 $\mu m^2$.

In the receiver (Rx) we use an EDFA to pre-amplify the signals before they are fed into a polarization-diversity intradyne system, the input power to which was kept constant throughout all measurements. A second fiber laser (laser 2) with a linewidth of approximately 200 Hz (centered at 1550 nm) serves as a local oscillator (LO). An Agilent N4391A optical modulation analyzer (OMA) is used to record the incoming signals. We slightly detune the bias of the modulator in the Tx and allow a residual carrier which serves as reference for frequency offset compensation. No additional pilot tone was sent over the link.

All digital signal processing (DSP) and signal evaluation was performed offline. The processing included chromatic dispersion compensation [18,19], separation of the two polarizations [20], channel equalization, and a new special zero roll-off clock phase recovery [2]. The sampled complex signals of X- and Y-polarization are equalized by an FIR filter which removes accumulated dispersion associated with the properties of used fiber spans. As a next step the signal is analyzed in the Stokes parameter space and aligned to the polarization axis of the receiver [20]. This algorithm does not compensate for polarization mode dispersion, and no feedback regarding the signal quality is given. The clock phase recovery assures that the signal is sampled at the point of maximum eye opening. Carrier phase recovery is performed by compensating a residual frequency offset of the signal, corresponding to a linear phase over time, in the frequency domain. Then the constellation diagram is aligned to the real- and imaginary axis of the OMA by minimizing the error vector magnitude (EVM). Finally, a linear FIR equalizer with 55 taps is trained through a feedback mechanism and optimizes the signal quality by minimizing the EVM. This equalizer removes

#161525 - $15.00 USD Received 13 Jan 2012; revised 18 Feb 2012; accepted 29 Feb 2012; published 5 Mar 2012

pattern effects as well as it compensates for the linear impulse response of the used components (DAC, modulator, ADC, and amplifiers). Non-linear algorithms (e. g. digital back propagation) have not been used.

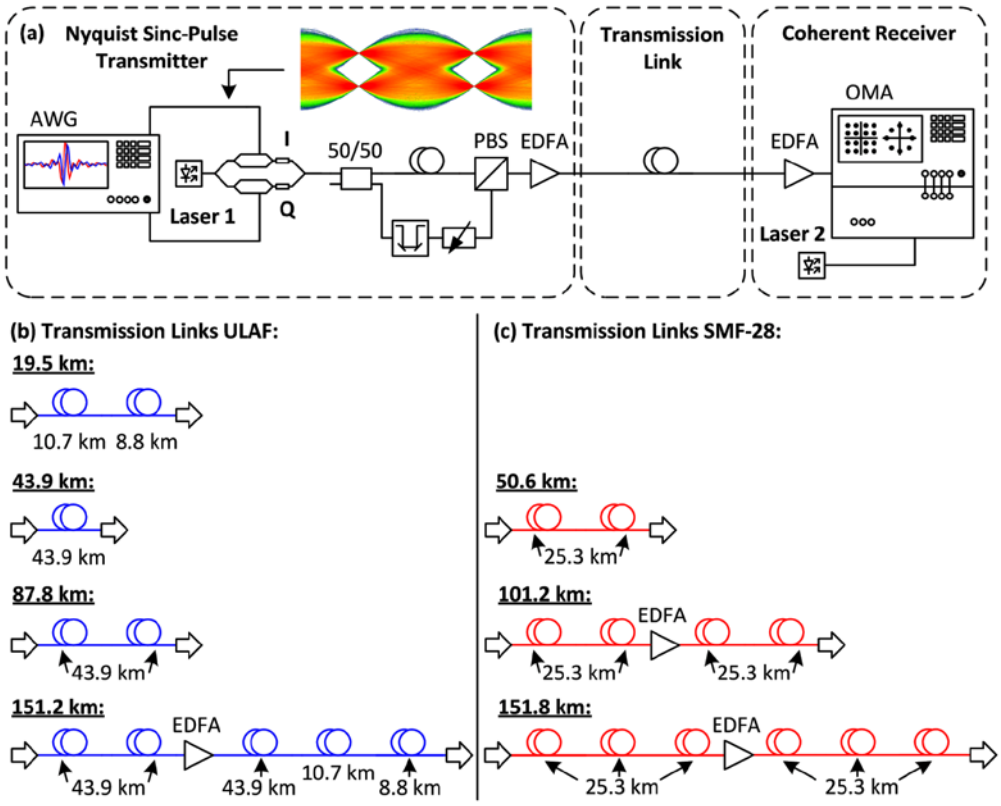


Fig. 2. Transmission setup. (**a**) An optical transmitter based on an Agilent arbitrary waveform generator (AWG) generates, with the help of a narrow-linewidth fiber laser (laser 1), a variety of Nyquist sinc-pulses. The inset shows a schematic eye-diagram for a two-level zero roll-off Nyquist signal. The optical signal is split, de-correlated, and recombined in orthogonal polarizations to emulate polarization division multiplexing (PDM). Several fiber spans are inserted in-between two EDFAs before the signal is received by an Agilent optical modulation analyzer (OMA) using a second narrow-linewidth fiber laser (laser 2). (**b**) Several ULAF based transmission links that were used for our experiments. (**c**) Several SSMF based transmission links that were used for our experiments.

## 3. Results

### *3.1 Performance compared to the Shannon limit*

The limiting capacity $C$ for error-less transmission over a linear channel with Gaussian distributed signal and additive white Gaussian noise (AWGN) is given by [21]

$$C = B\log_2(1+\mathrm{SNR}). \qquad (2)$$

The quantity $B$ denotes the channel bandwidth (here $B$ = 3 GHz; see Fig. 1(b)), and SNR is the signal-to-noise power ratio for Gaussian distributed signal and noise. For an SNR of 37 dB as measured with the coherent receiver for one polarization only, this limiting channel capacity amounts to $C$ = 37 Gbit/s. The maximum spectral efficiency $\mathrm{SE}_{\max}$ per polarization is obtained by relating the limiting channel capacity Eq. (2) to the channel bandwidth,

$$\mathrm{SE}_{\max} = C/B = \log_2(1+\mathrm{SNR}). \qquad (3)$$

#161525 - $15.00 USD Received 13 Jan 2012; revised 18 Feb 2012; accepted 29 Feb 2012; published 5 Mar 2012

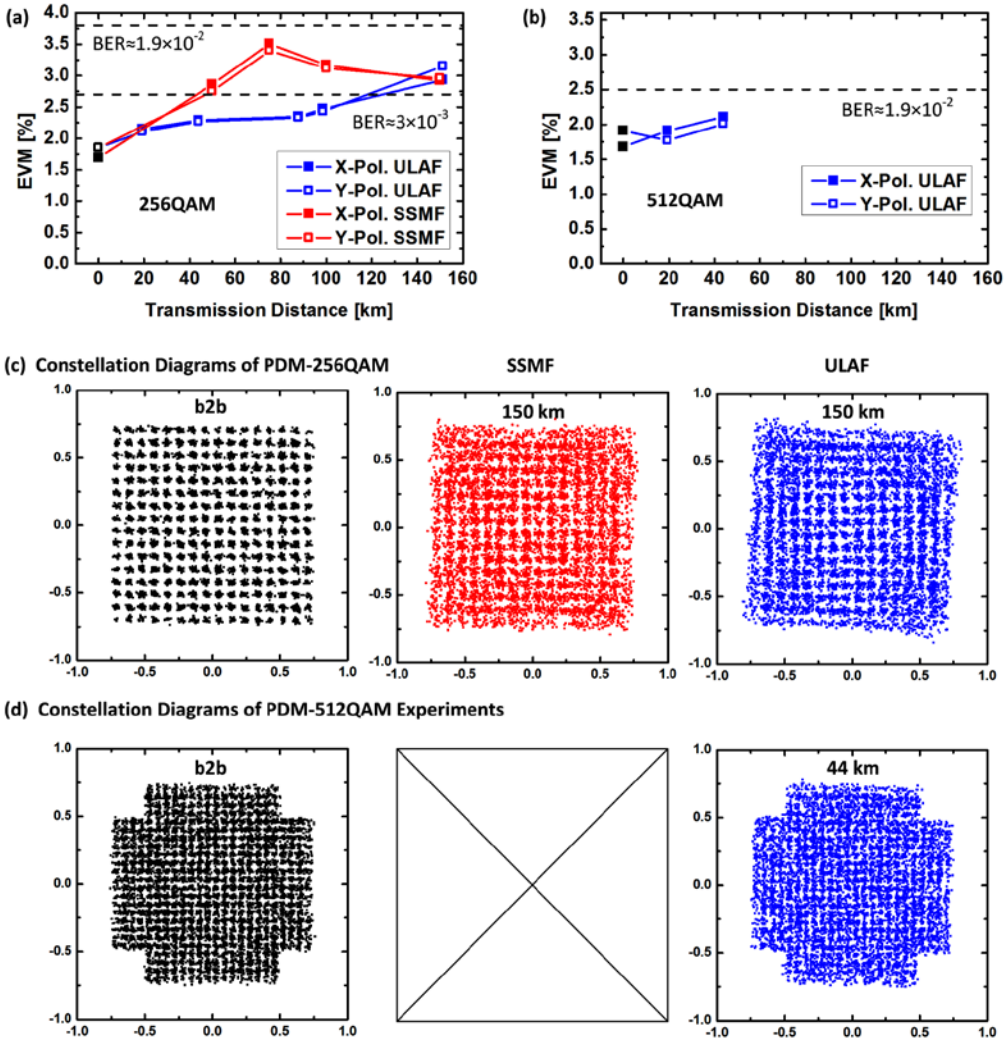


Fig. 3. Experimental results for transmitted 256QAM and 512QAM signals. The first row shows the measured EVM of the two polarizations transmitted over a SSMF (red), an ULAF (blue), and back-to-back (b2b) (black). Limits of BER suitable for error-free transmission employing state-of-the-art FEC algorithms are indicated by dashed horizontal lines. (**a**) EVM performance of Nyquist shaped PDM-256QAM data for different fiber spans. (**b**) EVM performance of sinc-shaped PDM-512QAM data for different fiber spans. (**c**) Constellation diagrams for PDM-256QAM and (**d**) PDM-512QAM signals. Both polarizations are plotted within a single constellation diagram. The color coding refers to the type of fiber used for transmission.

With the data above, a maximum $SE_{max}$ of 12.3 bit/s/Hz results per polarization. We actually measured 0.5 × 56 Gbit/s/3 GHz = 9 bit/s/Hz per polarization, i. e., 18 bit/s/Hz for PDM-512QAM data in a hypothetical WDM network, at a worst-case BER of $1.9 \times 10^{-2}$. To compare to the Shannon limit, we have to employ a forward-error correction (FEC) scheme with either 6.7% overhead for a BER up to $3 \times 10^{-3}$, yielding an effective BER of $10^{-16}$ [22], or a 25% overhead for BER up to $1.9 \times 10^{-2}$ resulting in an effective BER of $1.1 \times 10^{-15}$ [23]. The resulting BER are small enough to approximate an error-free transmission.

Consequently, our effective SE reduces from a raw value of 18 bit/s/Hz to $SE_{1.9 \times 10-2}$ = (18 / 1.25) = 14.4 bit/s/Hz and $SE_{3 \times 10-3}$ = (16 / 1.067) = 15 bit/s/Hz, respectively. After

#161525 - $15.00 USD Received 13 Jan 2012; revised 18 Feb 2012; accepted 29 Feb 2012; published 5 Mar 2012

transmission of these signals over 44 km of ULAF, a SNR = 36 dB is recorded. For two polarizations the Shannon limit then would be $2 \times SE_{max} = 2 \times 12$ bit/s/Hz according to Eq. (3), still significantly larger than our optimum $SE_{3 \times 10-3} = 15$ bit/s/Hz. Effectively, we are limited by receiver noise as the input power to the receiver was lower for transmission than in the back-to-back case.

*3.2 Signal quality evaluation for back-to-back and transmission experiments*

Measurements were performed for a transmission up to 150 km for 256QAM and up to 44 km for 512QAM using an ULAF and a SSMF fiber, respectively.

The first row of Fig. 3 shows error vector magnitude (EVM) plots as a function of the different transmission link lengths as depicted in Figs. 2(b) and 2(c). For a better legibility, dashed horizontal lines indicate bit error ratios (BER) calculated from the measured EVM [24] for common forward error correction (FEC) limits; see Figs. 3(a) and 3(b). Since we use random input data, a non-data-aided reception leading to the EVM metric is obligatory. A comment on the reliability in using EVM to estimate BER is to be found in the Appendix. All EVM are plotted for the two polarizations separately (solid and open symbols). Back-to-back measurements are black, SSMF related EVM data are colored red, and ULAF related measurements are colored blue. All received signals show EVM below the FEC limit having a BER equal to $1.9 \times 10^{-2}$.

The remaining two rows show the aggregate constellation diagrams for both polarizations. Constellations for back-to-back experiments and for transmission over 150 km of either SSMF or ULAF for the Nyquist shaped PDM-256QAM data are seen in Fig. 3(c). The constellation diagram for the 150 km ULAF link shows some non-linear distortions that we attribute to the relatively high launch power as well as imperfect carrier phase synchronization. Therefore, the estimation of the BER by EVM measurements shows some inaccuracy as will be discussed in Section 3.3. The signal performance in the SSMF fiber at 50 km and at 100 km could be improved with further optimization (e. g. by adjusting the launch powers into the fiber spans). The constellation diagrams for sinc-shaped PDM-512QAM Nyquist signals in the back-to-back case and for 44 km ULAF transmission is shown in Fig. 3(d). Transmission of the 512QAM format over a SSMF was not possible with a reasonable BER. For all measurements we tested the setup for its tolerance towards polarization rotation and found negligible influence on the signal quality.

*3.3 Statistical analysis of received data*

In order to verify the use of EVM, which requires that signal and noise are Gaussian distributed, we analyze the statistical properties of the received field vectors displayed in Fig. 3 with respect to their nominal positions. The deviations from each constellation point are the error vectors, which form a bell-shaped joint probability density function (PDF) as a function of real and imaginary parts of the error vector centered at the respective constellation points. Figure 4(a) shows two neighbored constellation points for the inphase (real part) of the electric field with the respective cross-section PDF in blue and red. We see that for non-data aided reception, as is employed in this work, a decision threshold is required to assign received data to the closest constellation point. This can lead to false assignments and therefore to an underestimation of EVM and BER. However, we already showed that for signals with $BER \leq 10^{-2}$ the EVM difference between non-data aided reception and data aided reception is negligible [24].

The statistics of the error vectors for all points in the constellations in Fig. 3 were individually checked. The PDF were Gaussian-like, but due to the relative small number of samples (< 100) for each constellation point not very smooth. For better judging how close to a bivariate Gaussian the joint PDF of the error vectors are, we collect all complex error vectors irrespective of the constellation points they were originally associated with. We also disregard the fact that the 61 (72) constellation points of the outermost rows and columns for 256QAM (512QAM) are more noisy than the dominant number of inner ones, which

#161525 - $15.00 USD Received 13 Jan 2012; revised 18 Feb 2012; accepted 29 Feb 2012; published 5 Mar 2012

represent a fraction of 76% (86%). We relate all error vectors to the field magnitude of the outermost point of the constellation under discussion. We then numerically integrate over the real-part of the error vectors to find the $PDF_i$ of the imaginary part, and repeat this procedure by numerically integrating over the imaginary-part of the error vector to find the $PDF_r$ of the real part. Both, $PDF_r$ and $PDF_i$, are superimposed and form one histogram, Fig. 4(b) and 4(c).

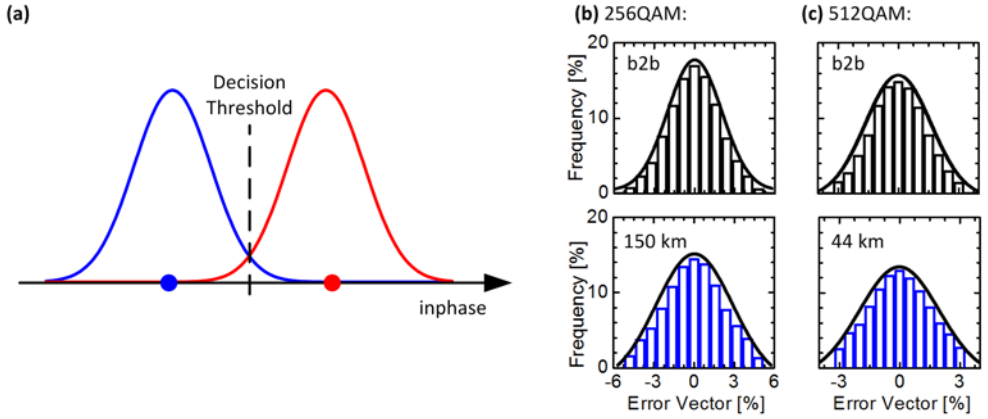


Fig. 4. Schematic and measured probability density functions (PDF) approximated by histograms of measured error vectors. (**a**) PDF of two neighboring symbols (blue and red) along the inphase axis for the real part of the electric field, along with their bell-shaped PDF of the error vectors. For non-data aided reception, the required decision threshold could lead to false symbol assignments. For BER ≤ $10^{-2}$ this effect is negligible [24]. (**b**) Histograms approximating a representative PDF both for real and imaginary part of all normalized error vectors of a 256QAM constellation diagram. Upper row: Back-to-back (b2b) transmission, lower row: 150 km ULAF. (**c**) Histograms approximating a representative PDF both for real and imaginary part of all normalized error vectors of a 512QAM constellation diagram. Upper row: Back-to-back (b2b) transmission, lower row: 44 km ULAF.

The frequency of occurrence in Figs. 4(b) and 4(c) is proportional $PDF_r$ + $PDF_i$ as discussed before and resembles a Gaussian closely, which is provided as a solid black fit curve. The respective decision thresholds are located at both the horizontal ends of the error vector axis. It is seen that here the Gaussian is virtually at zero so that interference from neighboring constellation points can be neglected, even for non-data aided reception as discussed in the beginning of this Section. Figures 4(b) and 4(c) show the results for back-to-back (b2b, upper row) and transmission over an ULAF with 150 km and 44 km length (lower row). These findings support the hypothesis of Gaussian noise dominating the signal quality. For the signal itself the Gaussian hypothesis can be safely assumed based on the central limit theorem. We can therefore use Eq. (4) to compute an equivalent BER from measured EVM as derived in [24],

$$BER \approx \frac{1-L^{-1}}{\log_2 L}\,\mathrm{erfc}\left[\sqrt{\frac{3\log_2 L}{\left(L^2-1\right)\left(k\ \mathrm{EVM_m}\right)^2 \log_2 M}}\right]. \qquad (4)$$

Here $L$ denotes the number of signal levels in each dimension (e. g. $L_{16QAM}$ = 4), and $\log_2 M$ is the number of bits encoded into each symbol. The conversion factor $k$ is used to convert EVM normalized by the outermost constellation point to the EVM defined by the average power. For 256QAM we find $k^2$ = 45 / 17, and for 512QAM $k^2$ = 529 / 165. Unfortunately we spotted a misprint in Eq. (4) of [24] where √2 has to be replaced by a 1. However, the corresponding plot in Fig. 3(b) of [24] has been calculated correctly.

#161525 - $15.00 USD Received 13 Jan 2012; revised 18 Feb 2012; accepted 29 Feb 2012; published 5 Mar 2012

## 4. Conclusion

In this paper we show for the first time the transmission of 54 Gbit/s within an optical bandwidth of only 3 GHz over 44 km of ULAF employing zero roll-off Nyquist pulse shaping. Furthermore, we demonstrate signals with a data rate of 48 Gbit/s and 3 GHz optical bandwidth transmitted over 150 km of SSMF while the achieved signal quality is still suitable for error-free transmission using state-of-the-art FEC. Negligible inter-channel crosstalk is expected when employing the demonstrated signals in Nyquist WDM networks as the out-of-band suppression is >36dB. This will lead to a potential SE of 18 bit/s/Hz (16 bit/s/Hz) without and a net SE of 14.4 bit/s/Hz (15 bit/s/Hz) with FEC overhead. Corrections with signals having BER $\leq 3 \times 10^{-3}$ require an FEC with 6.7% [22] overhead, but for BER $\leq 1.9 \times 10^{-2}$ FEC algorithms introducing 25% overhead [23] are required. As a result we find that transmission of PDM-256QAM signals leads to a higher net SE than transmitting PDM-512QAM data. The theoretical gain in SE of two bit per symbol is consumed by a decreased noise tolerance and by an increased FEC overhead.

## Appendix A

The relation between EVM and BER [24] is theoretically well understood and has been used long since in wireless communications. EVM and BER are mathematically correlated in systems dominated by additive Gaussian amplifier noise. In optical communication systems where signals are made up from a large number of symbols, the reach is typically limited by additive Gaussian noise from the amplifiers. Nonlinear noise is not likely to dominate – otherwise the small distance in field strength from one symbol to the other would no longer allow transmission over multiple amplifier stages. However, even in the presence of nonlinear effects, where neighboring optical channels cross-couple random signals to the channel under consideration, these nonlinear perturbations are effectively Gaussian in nature due to the central limit theorem as has been demonstrated in extended simulations of WDM systems with up to 32 channels [25, Fig. 7]. This is supported by findings that for narrowly spaced differentially phase shift keyed (DPSK) WDM systems, cross-phase modulation (XPM) contributes dominantly. However, XPM also adds noise with Gaussian statistic [26]. These ascertainments are supported by a number of experimental studies [2,8,24], where we proved the viability of this metric in optical communications. Even if there are some non-linear impairments degrading the signal quality such as phase noise or non-linear DSP, effects by Gaussian noise are usually dominant when measuring BER. As a consequence, soft-decision FEC can be applied to improve a raw BER of up to $1.9\times10^{-2}$ to an effective BER of $1.1\times10^{-15}$, at the expense of a 25% overhead [23]. In addition, recording complex error vectors allows to check the distribution of the noise [8] giving deeper insight into the nature of possible deficiencies, whereas BER measurements do not reveal any statistical information in that context.

## Acknowledgments

This work was supported by the EU projects ACCORDANCE and EuroFOS, the Agilent University Relations Program, the Polytec GmbH, OFS Norcross, the German BMBF project CONDOR, and by the Karlsruhe School of Optics & Photonics (KSOP).

#161525 - $15.00 USD Received 13 Jan 2012; revised 18 Feb 2012; accepted 29 Feb 2012; published 5 Mar 2012